NUMERICAL STUDY OF A CONTINUUM SONIC JET INTERACTING WITH A RAREFIED FLOW

by

Christopher E. Glass*
NASA Langley Research Center
Hampton, VA 23681-0001

and

Gerald J. LeBeau†
NASA Lyndon B. Johnson Space Center
Houston, TX 77058-3696

Abstract

The results of a numerical study with flow and boundary conditions based on an experiment of a continuum sonic jet interacting with rarefied flow about a sharp leading edge flat plate at zero incidence are presented. Comparisons are made between computational fluid dynamics (CFD) and direct simulation Monte Carlo (DSMC) solutions which provide an assessment of applying each technique to the flow conditions of the experiment. An analysis of the CFD results revealed a correlation between the interaction interface of the jet continuum breakdown surface and a non-dimensional parameter derived from jet and free stream flow conditions. Using the breakdown surface from the correlation, the continuum jet was uncoupled from the interaction, thus allowing an uncoupled CFD-DSMC solution to be obtained. Also, a nearest neighbor collision algorithm, similar to the sub-cell technique, was implemented in the DSMC solution technique. The comparison between CFD and DSMC results shows good qualitative agreement in the interaction region and good quantitative agreement elsewhere.

Nomenclature

d	molecular diameter [m]
dia	diameter [m]
G	non-dimensional parameter
k	Boltzmann's constant
Kn	Knudsen number
m	molecular mass [kg]
n	number density [molecules/m^3]
n_o	Loschmidt's number
L	characteristic length [m]
M	Mach number
N	inverse of breakdown parameter, P
p	pressure [Pa]
P	breakdown parameter
$\dot{q}''$	heat flux [W/m^2]
T	temperature [K]
V	velocity with components u,v,w [m/sec]
x,y,z	Cartesian coordinate system
λ	mean free path [m]
ρ	density [kg/m^3]
τ	characteristic time [sec]
ν	intermolecular collision frequency [1/sec]

Subscripts

jet	sonic jet condition
∞	free stream condition

Introduction

As a vehicle enters an atmosphere, either to deorbit or to accomplish an orbital aerobrake maneuver, active control is provided by the vehicle reaction control system (RCS). For example, as the Shuttle Orbiter leaves orbit for an atmospheric entry, the RCS is the only vehicle control mechanism. After passing through

* Research Engineer, Aerothermodynamics Branch, Aero- and Gas-Dynamics Division. Member AIAA.

† Research Engineer, Aeroscience Branch, Aeroscience and Flight Mechanics Division.

Copyright © 1997 by the American Institute of Aeronautics and Astronautics, Inc. No copyright is asserted in the United States under Title 17, U. S. Code. The U. S. Government has a royalty-free license to exercise all rights under the copyright claimed herein for Governmental purposes. All other rights are reserved by the copyright owner.

the free molecular regime during entry, the Shuttle Orbiter enters the rarefied flow regime. The number density of the free stream increases with decreasing altitude and the RCS begins to interact with the flow. The RCS provides vehicle control for the Shuttle Orbiter through the transition from the rarefied to the continuum regime until the aerodynamic control surfaces (elevons, body flaps, rudder, etc.) become effective trim devices. In fact, the aft yaw RCS jets are required for trim from early entry in the atmosphere down to flight speeds of about Mach number one[1]. Early experience with the Shuttle Orbiter showed that the RCS jet interaction correlations from conventional wind tunnel tests marginally predicted hypersonic aerodynamic flight characteristics in the rarefied and near rarefied continuum regimes. (For example, see Refs. 1 and 2 for a thorough discussion of this subject.)

The NASA Shuttle Orbiter has been operational for just over 1½ decades using technologies developed nearly thirty years ago. In an effort to ensure reliable and affordable future access to space for the nation, the NASA is developing new technologies for a next generation single-stage-to-orbit (SSTO) reusable launch vehicle (RLV)[3]. The RLV is planned to replace the current space transportation system.

The RLV will clearly need a RCS during orbital maneuvers and during atmospheric entry at the end of a mission. The effects of the RCS jet interaction on the Shuttle Orbiter aerodynamic characteristics is well known by experience throughout the flight profile; however, these effects are configuration specific and the extensive database is not applicable to other vehicle classes. Therefore, studies of the RCS interaction effects applicable to the RLV configuration should be undertaken. Of interest are RCS interactions during entry through the rarefied and near rarefied continuum flow regimes where correlations from conventional wind tunnels may need to be refined by results from numerical studies to provide an adequate flight aerodynamic database.

Also, planetary probes, such as the Magellan and Mars Global Surveyor (MGS), have or will use RCS in a rarefied environment during the aerobraking phase of their missions[4,5]. A Planetary Exploration Program has been established and the MGS is the first of a series of orbiters and landers of the Mars Surveyor Program. A pair of spacecraft is planned to be sent every twenty six months to Mars for the next five years. The next surveyor missions are the Mars ‘98 and the Mars ‘01; the Mars ‘98 is being built. Both the MGS and Mars ‘98 will be actively controlled by RCS during aerobraking maneuvers to change the vehicle orbit about Mars. Although specific aerodynamic characteristics of planetary aerobraking in the rarefied regime for some probes have been studied[4,5], more studies are necessary to quantify aerobraking vehicle aerodynamics for future planetary missions.

Thus, a need exists to accurately model and understand RCS interactions in the rarefied flow regime for both the next generation SSTO vehicle and upcoming planetary exploration probes. The current research provides fundamental understanding of jet interactions in rarefied flow, develops numerical strategies that can be applied to geometry specific problems, and is needed to meet critical milestones of upcoming programs.

Problem Description

Some dependence must be placed on numerical simulations to describe the effects of RCS interactions on vehicle aerodynamics during hypersonic flight in the rarefied regime because correlations from conventional wind tunnels may not adequately predict the flight characteristics. To validate the numerical techniques, comparisons with results from available low density experimental studies must be made. Several experimental and computational jet interaction studies relevant to RCS interactions in the rarefied regime have been accomplished recently for flow in low density perfect gas environments for simple geometries[6-10]. However, more of these jet interaction comparisons are required to gain greater confidence in the capability of existing numerical techniques and to set limits of technique applicability for studies of RCS interactions for RLV entry, planetary aerobraking, and other missions in the rarefied flow regime.

An experimental study of a jet interaction with rarefied flow over a sharp leading edge planar surface at zero incidence has recently been completed in the Low Density Tunnel (LDT) at the Defense Research Agency (DRA) in Farnborough, United Kingdom by Warburton[8]. When published, the study will provide experimental results to compare with numerical capabilities for a perfect gas jet interaction simulation. The free stream flow of the experiment has a mean free path, $\lambda \approx 0.2$ mm. The altitude with an equivalent mean free path is about 60 kilometers above the Earth surface[11]. The Knudsen number, Kn, is 0.05 when based on the free stream mean free path and the orifice diameter. This Knudsen number is at the overlap between the continuum and rarefied flow regimes.

A sketch showing pertinent geometric dimensions of the flat plate model used for the experimental study is shown in Fig. 1. Heated nitrogen gas is expanded to provide a free stream flow at a nominal Mach number of 9.84, static temperature of 65K, and static pressure of 5.4 Pa for the experiment. Four jet gases were used during the experiment: helium, nitrogen, argon, and carbon dioxide at plenum or total temperature of 300K

and plenum or total pressures of 17.4, 34.5, and 51.7 kPa. The jet was expanded from a plenum to a sonic condition at the nozzle exit and released perpendicular to the flat plate surface. The experimental study offers a unique opportunity to study a jet interaction with both CFD and DSMC solution techniques because the free stream flow is rarefied and the interacting jet is continuum.

The three-dimensional numerical study presented in this paper utilizes the geometry and test conditions of the free stream and jet of the experiment. Although CFD solutions for all twelve cases have been accomplished, detailed CFD results of only the interaction of the argon jet with a corresponding plenum pressure of 34.5 kPa are given because one of the main purposes of this study is to establish applicability limits of the CFD and DSMC techniques for the jet interaction problem. To this end, a comparison of CFD and DSMC results from one of the jet interaction cases is given.

Computational Methods

CFD for this study is provided by the General Aerodynamic Simulation Program[12,13] (GASP), a commercially available software product of AeroSoft, Inc. The GASP is a three-dimensional finite-volume flow solver based on the Reynolds averaged Navier-Stokes equations. The program has options of solving two-equation turbulence models and flows with non-equilibrium chemistry and non-equilibrium internal energy.

The DSMC technique is also applied for the numerical jet interaction study. The direct simulation Monte Carlo (DSMC) method is valid for any flow field simulation with a dilute gas that is not influenced by a highly ionized plasma because it is based directly on relationships, which form the basis of the kinetic theory of gases[14,15]. The DSMC technique does not solve a set of equations to produce a solution of the flow field, but rather statistically tracks movements and collisions of simulated molecules, each of which represent an average of many molecules. The velocity and position of simulated molecules are allowed to change within and through the boundaries of a fixed number of cells in a discretized computation space as time is advanced. Statistical probability determines post collision velocity of interacting molecules. After many time steps, average macroscopic gas properties of the simulated molecules in each cell produce a flow solution within the boundaries of the domain. Likewise, surface properties are determined by averaging many molecular wall collisions, which exchange momentum and energy at the wall boundary. (See Refs. 14 and 15 for a complete description of the technique.)

The DSMC Analysis Code (DAC) of LeBeau[16] is used to apply the DSMC simulation for the present study. The Borgnakke and Larson[17] model is used in the DAC to account for energy transfer between kinetic and molecular internal energy modes. Domain boundaries of vacuum, free stream, and symmetry, and wall boundaries of solid, outgassing, inflow, and outflow are currently available. Multiple specie simulations with variable wall molecular reflectivity and variable temperature are also available. The DAC is presently a beta version research computer program under development and references for the program are few; however, early results are quite promising. Results reported in Ref. 16 show good agreement between DAC and other DSMC implementations.

The DAC execution program is written with message passing interface[18] (MPI) subroutine calls in the software algorithms, which allows it to take advantage of memory and parallel processing capabilities of program execution on multiprocessor and multiple-networked computers. For the present study, DAC employs the use of the Local Area Multicomputer[19] (LAM) version of MPI to provide code execution on local SGI workstations with R10000 processors.

Discussion and Results

Two types of flow solutions are presented for the jet interaction problem: a complete CFD solution and a uncoupled CFD-DSMC solution. The CFD solution of the interacting flow is from a direct application of the GASP[13] computer program to the given boundary conditions of the problem. The approach taken to produce a DSMC solution is to uncouple the jet continuum region from the rest of the external flow field and solve the interacting flow by the DSMC method. By uncoupling the jet flow, a molecular simulation is not applied to the high density jet plume outside the nozzle exit, thus reducing computational requirements. However, the difficulty for the uncoupled CFD-DSMC solution is defining the location where the jet begins to interact with the rarefied free stream to avoid a coupled CFD-DSMC solution. The complete CFD flow solutions are analyzed to determine the jet interface with the interaction region. Presented below is a discussion of the specific details of applying the two computational methods, the analysis of the CFD solutions, and a comparison of the results obtained.

Computational Fluid Dynamics

An isometric drawing showing the volume of the CFD numerical domain is given in Fig. 2. The domain extends 0.1 m behind the flat plate and includes the

region under the plate. Any effect on the upper flat plate flow from the lower plate wake influence should be captured by including the lower plate and wake regions in the computational domain. Additionally, the computational domain includes the subsonic portion of the nozzle from the plenum chamber to the nozzle exit on the flat plate surface. Because the nozzle has a no slip wall boundary condition that provides for nozzle boundary layer development, the flow injected out through the nozzle exit is properly modeled. The flat plate is 0.150 m long and 0.210 m wide; however, because symmetry exists along the x-z plane midway of the plate, only one-half on the flow field was modeled computationally. Fig. 2 shows the x-z plane of symmetry.

The CFD domain contains six zones (also called blocks). By dividing the domain into smaller regions, less computer memory resources are used when processing a solution as compared to a domain without such a multi-zone (or multi-block) arrangement. The multi-zone arrangement also allowed for the nozzle zone and zone above the nozzle, which are constructed using a cylindrical coordinate system, to be connected to adjacent zones described by a Cartesian coordinate system. A total of 319,488 cells are used to describe the flow domain, the maximum number of cells in any one zone is 98,304. During the numerical time integration of a solution, flux vector information was allowed to pass in both directions between boundaries of zones to ensure no information was lost between zones.

The number of cells in each direction of a zone is divisible by four to allow mesh sequencing to be applied to the computation solution. Within the structure of the GASP CFD program, a coarse mesh solution can be interpolated as an initial condition to a fine mesh. For the jet interaction problem, three levels of mesh sequencing are used. Mesh sequencing can drastically reduce the time required to iterate a CFD solution to convergence[12,13].

The computational solution from the GASP requires inviscid and viscous flux models, chemistry, and boundary conditions be specified. The inviscid flux scheme of Roe is applied to the nozzle zone, and the inviscid flux scheme of Van Leer is applied to all other zones. Flux limiting is accomplished using the method of Van Albada with third order upwind biased spatial accuracy. The laminar viscous flux model with all thin layer and cross flow terms (full Navier Stokes approximation) is applied for the solution scheme. A second order accurate wall gradient calculation applies to wall calculated quantities (that is, heat flux, skin friction, etc.). Sutherland's law with Wilke's mixing model specifies viscosity and conductivity transport properties for closure of the momentum and energy equations. Flow chemistry is modeled as two specie frozen mixture in translational and rotational equilibrium. The nozzle gas is modeled as one species and the free stream gas as the other species even when both gases are the same. The solid wall boundary conditions of temperature at 300K and no slip are applied to all zones in contact with the flat plate or nozzle. All outflow boundaries are calculated as first order extrapolated from the interior of the domain.

Solutions were obtained using global iterations of all zones with mesh sequencing and convergence was based on the value of the solution L_2 norm. The L_2 norm provides a measure of numerical convergence by showing the root mean squared difference between flux values of two consecutive iterative steps normalized by the flux values assigned to the grid prior to starting the numerical solution. After the L_2 norm decreased to a value of about $1x10^{-9}$ based on the initial condition, the solution was assumed converged as the L_2 norm no longer decreased and the change between iterations was judged close to machine round-off error. Each CFD solution for the present study was accomplished on a single processor of the decommissioned NASA Langley Cray Y-MP supercomputer (Sabre) using about 5.5 million words (Mwords) of random access memory (RAM) for the fine grid time integration and required about sixty hours to reach the level of L_2 norm convergence indicated above.

Fig. 3 shows the flow field streamlines for the CFD solution of the argon jet interaction with a jet plenum pressure of 34.5 kPa. Since the CFD solution was integrated numerically to a steady state condition, the arrowed lines on the figure represent flow streamlines. Each streamline is tangent to the flow field vector by which it passes and traces the path of a fluid element through the flow field. The free stream flow is from left to right, and the sonic argon jet is injected normally through a nozzle located 0.125 m downstream of the flat plate leading edge on the upper flat plate surface.

Normalized number density at the symmetry plane for the argon jet interaction flow field is shown next in Fig. 4. The number density is normalized by Loschmidt's number, n_o, where $n_o = 2.68666 \times 10^{25}$ molecules/m^3. Loschmidt's number, or standard number density, is the number density of ideal air at standard temperature and pressure (STP)[15]. A more through discussion of the CFD results will be presented below in the section entitled Comparison between CFD and DSMC where jet interaction results from the two numerical techniques are compared.

Breakdown of the Continuum Jet

For the uncoupled CFD-DSMC jet interaction solution, the approach is to define the boundary

between continuum jet and free stream interacting flow similar to that of a breakdown surface. To determine the departure of an expanding flow, such as the jet, from a continuum flow condition, Bird[15] proposes that a breakdown surface be defined with an associated breakdown parameter, P, of numerical value 0.02. In this section the theory and mechanics of producing a breakdown surface from known flow field quantities, such as from a CFD solution, are developed and presented.

The approach for modeling the jet plume for the present study is similar to one that has been applied previously to study free expanding plume impingement[20,21]. The jet plume of that study was modeled using a CFD solution; then, a breakdown surface and flow properties at the breakdown surface were derived from the CFD solution. Outside the breakdown surface, DSMC was applied with the breakdown surface as an inflow boundary to a molecular simulation.

In a study of expanding jet flow from the Shuttle Orbiter Primary Reaction Control System (PRCS) thrusters[21], a parameter, N, was used to determine the boundary between the continuum and rarefied regime. The parameter is given as:

$$N = \nu\tau \qquad (1)$$

where ν is the frequency of intermolecular collisions and τ is a characteristic time between collisions in the jet plume. Therefore, N is the number of intermolecular collisions in a characteristic time. Expanding the definition further, Ref. 21 gives the characteristic time as:

$$\tau = \frac{L}{V} \qquad (2)$$

with length, L, defined as:

$$L = \frac{\rho}{\nabla\rho} \qquad (3)$$

where ρ is the local density of the gas. Therefore, substituting Eqs. (2) and (3) into Eq. (1):

$$N = \frac{\nu\rho}{\vec{V}\cdot\nabla\rho} \qquad (4)$$

Also, the breakdown parameter, P, of Ref. 15 is related to the parameter, N, by:

$$P = \frac{1}{N} = \frac{\vec{V}\cdot\nabla\rho}{\nu\rho} \qquad (5)$$

Using definitions given in Ref. 15, the intermolecular collision frequency, ν, can be expressed as:

$$\nu = \left(\pi d^2 n\right)\left(\frac{16kT}{\pi m}\right)^{1/2} \qquad (6)$$

Eq. 5 provides a formulation for the breakdown parameter as a function of flow field variables. The breakdown parameter, P, can be calculated from a CFD solution of an expanding flow. The only variable in Eq. (5) that is not available from a CFD solution is the intermolecular collision frequency, ν, which is defined by Eq. (6).

For application to the jet interaction with a rarefied flow field, it will be shown that the value of P chosen to describe the extent of the breakdown surface is sensitive to a combination of jet and free stream conditions. The difficulty is to define the boundary between the two regions to optimize the use of both CFD and DSMC numerical techniques.

Analysis of the Breakdown Surface

Given the definition of the breakdown parameter, a scheme is implemented to calculate the breakdown surface from the jet interaction CFD solutions. A computer program that applies Eq. (5) to a PLOT3D[22] formatted CFD flow field solution file has been written. (PLOT3D is a common file format to represent a CFD grid and solution.) A central differencing operator in the program calculates the density gradient term except at boundaries where a single-sided operator is used. The mass and diameter of the expanding gas specie molecule are supplied as an input to the program. The output of the program is a PLOT3D formatted solution file containing the breakdown parameter, P.

A breakdown surface can then be obtained from the breakdown parameter solution file as an isosurface to define the geometry of the breakdown surface for a given value of P. A commercially available flow visualization and analysis program, EnSight™ (See Ref. 23.), is used to produce an isosurface corresponding to a constant value of breakdown parameter. An isosurface is created with the EnSight™ program by interpolation between the appropriately valued grid cell edges to define a point on the cell face. Points with the desired isovalue are connected and displayed as triangulated surface elements. The program provides,

as an ASCII text output file, the cloud of points, which spatially describe the geometry of a given isosurface. For the present study, the cloud of points are the spatial boundary points of the Bird breakdown surface for a given value of the breakdown parameter.

This technique was applied to PLOT3D solution files of the twelve CFD jet interaction cases for various isosurface values. As an example, results of analyzing the calculated breakdown parameter field for the argon jet interaction with a jet plenum pressure of 34.5 kPa are shown in Fig. 5. Isosurfaces at two values of the breakdown parameter are shown on the figure. At P = 0.01, the surface appears as a smooth body of revolution normal to the plane of the plate surface even though the breakdown parameter was calculated from a CFD solution of a complex jet interaction. (See Figs. 3 and 4.) At P = 0.02, however, the breakdown surface extends further from the plate surface and interfaces with the free stream interaction region. This is shown as a nearly diagonal jagged cut through the upper portion of the breakdown surface. The irregularity of the cut is because a gradient type operation is used by the flow visualization program to produce the isosurface from the breakdown parameter solution file, which is obtained by applying a gradient operator (Eq. (6)) to the flow field solution. Effectively, a Laplacian operation has been applied to discrete flow field values of the CFD solution and produces the irregular cut shown on the breakdown surface for the P = 0.02 case in Fig. 5.

For each interaction case analyzed, the breakdown parameter was varied to identify the value when the breakdown surface changed from a regularly shaped body of revolution to a body of revolution with a diagonal cut. The breakdown parameter value at the change shows the interface of the expanding jet with the free stream interaction.

Because the breakdown parameter value at the interface differed with jet gas type and jet plenum pressure, a correlation using the breakdown parameter values at the interaction interface was sought. To derive the correlating parameter, it was assumed that the physical mechanism active at the interface between the jet and free stream interaction was a ratio of flux-based quantities. By dimensional analysis, a ratio of the number density flux, nV, with the molecular collision probability flux, $\nu/(\lambda d)$, was found to provide a correlation with the breakdown parameter value at the interaction interface. The non-dimensional correlation parameter, G, is given as:

$$G = \frac{nV}{\left(\frac{\nu}{\lambda d}\right)} \qquad (7)$$

where n is the number density, V is the characteristic flow velocity, ν is the collision frequency, λ is the mean free path, and d is the molecular diameter. Note that the molecular quantities of Eq. (7) are taken as the hard sphere values for convenience.

Fig. 6 shows the relationship of the breakdown parameter, which corresponds to the breakdown surface at the jet interaction interface as a function of the non-dimensional parameter, G_{jet}/G_{∞}. Free stream influence on the relationship is obtained by normalizing the non-dimensional jet number, G_{jet}, at the jet gas nozzle exit conditions, by a non-dimensional free stream number, G_{∞}, at the free stream gas conditions. Shown on Fig. 6 as symbols are the breakdown parameter values from the twelve jet interaction CFD solutions at the interface. These results span the transition from the continuum to rarefied regime based on the continuum breakdown criteria defined in Ref. 15 (P = 0.02), which is included on Fig. 6 as a dashed line. Above the dashed line, expanding flow at the breakdown surface is rarefied; whereas, below the dashed line, the expanding flow is continuum.

A solid line is drawn through the symbols in Fig. 6. Although scatter exists between the symbols and the solid line, a general boundary between the undisturbed jet breakdown surface (region to the lower right of the solid line) and the interacting jet breakdown surface (to the upper left of the solid line) is shown in the figure. For example, the interface of the carbon dioxide jet surface with the free stream interaction occurs in the continuum regime, but the interface of the helium jet breakdown surface with the interaction occurs in a more rarefied regime. The solid line in Fig. 6 is significant because it shows that a breakdown surface corresponding to a breakdown parameter value (P) in the region to the lower right of the curve has not been disturbed by the interaction. Thus, the expanding jet flow can be uncoupled from interaction at that breakdown parameter value. By uncoupling the jet flow from the interaction, a continuum flow solution of the jet can be separated from a molecular flow solution of the free stream and interaction region.

A more general correlation, including effects of wall curvature, nozzle orientation with respect to the surface and free stream, etc., that defines the interaction interface for the case of complex geometric configurations may exist. However, for the present flat plate configuration, the correlation of breakdown parameter at the interaction interface with the non-dimensional parameter G_{jet}/G_{∞} shown in Fig. 6 can be made.

Direct Simulation Monte Carlo

Implementation of the molecular simulation of the jet interaction by the DSMC is discussed in this section. The DSMC method for the present study is applied by the DAC[16]. The DAC is not a single DSMC solution program but rather a series of computer programs -- a geometry, grid, and boundary condition preprocessor (predac); a program to execute the simulation (dac), and solution postprocessors (slice and sprop). (In parenthesis are the DAC executable names.) A detailed discussion of the steps used to produce the DSMC solution for the jet interaction problem is given next.

The uncoupled solution for the jet interaction first requires a CFD solution for the expanding jet. The jet is modeled as an axi-symmetric free expanding jet. The expanding jet solution is obtained by the GASP computer program used previously for the full CFD interacting jet solution. Although the GASP program is a finite volume three-dimensional CFD solver, two-dimensional and axi-symmetric solutions can be obtained by defining the computational domain with two symmetric grid planes and appropriate symmetry boundary conditions on the planes[12,13]. This was done for the present axi-symmetric expanding jet solutions. The GASP expanding jet solutions used the full Reynolds averaged Navier Stokes equations.

Modeling of the axi-symmetric nozzle is similar to the nozzle modeling for the interacting jet cases. That is, flow at the plenum temperature and pressure was allowed to expand through a converging nozzle to the sonic condition at the exit. However, rather than interacting with a free stream flow, the jet flow from the nozzle exit was allowed to expand further as a plume into an outer computational domain, which simulated an infinite vacuum. A first order extrapolation from the interior was specified as the outflow boundary condition for the computational domain. Wall temperature was held constant at 300K and a no slip condition was applied to the nozzle and outer region walls.

One of the symmetry grid planes of the computational domain for the expanding axi-symmetric jet is shown on the left side of Fig. 7. Shown on the right side of the figure are normalized number density contours of the CFD solution. Note that along the outflow boundary, the number density is reduced by at least four orders of magnitude from the plenum condition. The extent of the upper computational zone was chosen so that the expanding jet transitioned from continuum to rarefied flow before reaching the outflow boundary. This assured that a breakdown surface could be defined within the computational domain.

A breakdown surface for the expanding jet is obtained from the CFD solution, which was first processed to produce a breakdown parameter PLOT3D solution file. The breakdown parameter value was chosen so that the isosurface did not extend into the jet interaction interface region based on results from Fig. 6. A value of P = 0.01 fit this criteria. An analysis of breakdown parameter file by the EnSight™ program[23] provides the isosurface geometry as a cloud of points.

Although the pointwise description given by the EnSight™ program correctly maps the isosurface, the format is not compatible as a DAC surface description. The preprocessor program of the DAC requires the user to describe the geometry of the body for the DSMC study as groups of triangulated surfaces. To create the geometry file for the present solution, the flat plate geometry and the breakdown surface must be merged together in a format readable by the DAC preprocessor program.

Several software packages were required to process the geometry of the flat plate model and jet isosurface to produce the proper triangulated format. First, the cloud of points representation of isosurface was transformed to an initial graphics exchange specification (IGES) format[24]. The IGES format is common for most computer aided design (CAD) programs. A commercially available software program, Surfacer[25], was utilized to produce IGES formatted surface description.

To create the geometry of the flat plate model and combine it with the jet isosurface, another computer program, GridTool[26], was used. GridTool allows geometric descriptions of different formats (IGES, GRIDGEN, LaWGS, PLOT3D) to be merged together with geometries created from within the GridTool program. The program generates a group of surface patches with the same format that describe the entire surface geometry of interest. For the present study, the flat plate geometry, created within the GridTool program, was merged with the IGES jet isosurface obtained from the Surfacer program. A FELISA[27] input file is generated as an output option of the GridTool program. FELISA is an unstructured finite element volume grid generation program. (See Ref. 27 for a complete discussion of FELISA.) For the present application; however, only the FELISA surface triangulation routine was used. Triangulation density of the surface is controlled by distributing sources with the GridTool program, which are read by the FELISA surface routine.

One final step was necessary to provide a compatible DAC formatted surface description. An author written translation and boundary condition application computer program, ftodac, was applied to the FELISA output file. All surface points, the number of triangles of the surface, and triangle connectivity are rewritten from a FELISA to DAC type format by ftodac. Additionally, appropriate solid wall and jet

isosurface boundary conditions are assigned to the surface points. All solid walls of the flat plate are treated as noncatalytic, fully diffuse surfaces with full momentum accommodation. The jet isosurface is treated as an outgassing boundary with number density, velocity, and temperature of the jet assigned to the boundary. The outgassing boundary condition also assures that molecules moving toward the surface are allowed to pass out of the DSMC domain and not be considered for further collisions. Boundary conditions for the jet isosurface are interpolated from the original structured grid GASP PLOT3D solution file by a weighted distance squared subroutine of the ftodac program.

Shown in Fig. 8 is the triangulated surface description of the flat plate and jet isosurface for the argon jet interaction problem that was generated by the ftodac program. In the right upper corner of the figure is a close-up view of the argon jet outgassing surface. Note the dense surface triangulation of the surface. The closely spaced triangles allow a more detailed geometric and boundary condition description of the jet outgassing surface.

After the geometry and boundary conditions of the surface for the molecule simulation are defined, the DSMC domain size and boundary conditions must be specified. The DSMC domain size was chosen to entirely surround the flat plate model to simulate the experimental conditions more closely than if just the upper portion of the plate flow field were modeled. The extent of the DSMC domain is shown in Fig. 9. A free stream boundary condition is applied to all domain boundary faces except the symmetry plane where a symmetry boundary condition was applied.

To produce the DSMC solution, a grid adaptation scheme is used. The predac program of the DAC series generates a uniform Cartesian grid of level 1 cells for the initial molecular simulation. Triangulated surfaces that model the geometry clip into the Cartesian grid, and the appropriate body boundary conditions are applied to the clipped cells. The uniform grid solution resolves large scale flow field features. Level 2 cells with close grid spacing in regions of high number density are generated from the uniform grid solution. Level 2 cell spacing within level 1 cells is controlled by user input to the predac program. The grid adaptation process can be applied to a previously adapted grid.

A uniform grid and two adaptation grid cycles were applied to produce the DSMC jet interaction solution. The uniform Cartesian grid for the simulation is shown in Fig. 9. Two planes of the Cartesian grid are shown: a cross flow grid that intersects with the jet breakdown surface and a streamwise grid along the symmetry plane. The flat plate is shown in the figure shaded gray and the breakdown surface is shaded black.

The uniform Cartesian grid consisted of forty thousand cells; however, the volume of the flat plate and breakdown surface clip out about three thousand cells of the domain resulting in about 37,000 active cells for the simulation. About 430,000 simulated molecules were necessary to fill the cells with a average of about ten molecules per cell. After an initial transient period to equalize the number of inflow and outflow molecules in the DSMC domain, approximately ten thousand move cycles per molecule were made before the simulation was stopped. The uniform grid simulation required ten Mwords of computer memory and ran for 15.8 node hours using SGI R10000 CPUs.

Number density contours from the uniform grid solution are shown in Fig. 10. The number density contours reveal the large scale features of the flow field. Upper and lower plate shock waves that originate at the plate leading edge, the higher number density region near the jet outgassing surface, and the low number density region in the wake downstream of the flat plate are shown in the figure. Also note that these same features are shown in CFD solution presented in Fig. 4.

Based on the uniform grid solution, an adapted grid was produced with the same number of level 1 cells; however, the adaptation process allowed level 2 cells (inner cells) to be created within the level 1 cells. The resulting DSMC domain consisted of about 1,400,000 level 2 cells with about sixty thousand cells clipped out because of the volume occupied by the flat plate and breakdown surface. A DSMC solution was then executed using the adapted grid. Simulated molecules within the cells of the DSMC domain numbered about eleven million. The simulation was stopped after ten thousand move cycles per molecule once a steady condition was met, required 190 Mwords of computer memory, and executed for 421.5 node hours on SGI R10000 CPUs.

Another grid adaptation, based on the results from the first adapted grid simulation, was performed. The number of level 1 cells was increased by a factor of 2 in the x-y plane (plane of the upper flat plate surface) and by a factor of 5 normal to the flat plate surface. This choice was made to better resolve the plate boundary layer and forward jet separation region normal to the wall of the plate with level 1 cells. Two planes of the grid that resulted from the second adaptation are shown in Fig. 11. The DSMC domain for the second adaptation consists of 2,400,000 level 2 cells with 140,000 cells clipped because of the volume occupied by the flat plate and jet plume to the outgassing surface. A simulation was performed on the second adapted grid, which required 17,500,000 molecules and 375 Mwords of computer memory. Computer execution time was 795.9 node hours on SGI R10000 CPUs, and

the execution was stopped after ten thousand steady state moves per molecule.

The second adapted grid solution lacked proper grid spacing for cells near the surface. Cell size normal to the wall ranged from about four mean free paths over the forward portion of the plate to nearly ten mean free paths in the higher density interaction region. Cell dimension normal to the wall is much larger than the sub-mean free path value recommended in Ref. 28 to resolve surface properties for hypersonic viscous interactions. For the present simulation, inadequate cell spacing was unavoidable because the number of molecules required for mean free path or less dimensioned cells normal to the wall would increase the problem size over an order of magnitude greater than the size of the present second grid adaptation case and computational resources are not available locally for such sized simulations. It was also shown in Ref. 28 that inadequate cell resolution normal to the wall results in higher heating predictions. This was the case with the second adapted DSMC solution when compared to the CFD solution. When cells near the wall are too large, momentum and energy transfer is higher because simulated molecules have not experienced enough molecular collisions to approach a local equilibrium prior to encountering the wall.

To improve the simulation accuracy of the second adapted grid, the collision sorting routine of the DAC was modified to allow nearest neighbors within a cell at the same normal distance from the flat plate surface to have a higher probability of collision. This is similar to the sub-cell methodology of Ref. 15. Also, the global time step of the simulation was decreased by an order of magnitude to restrict molecular movement and take greater advantage of the nearest neighbor modification to the molecule sorting routine. This change allows more molecular collisions before a molecule encounters the wall.

With the above modification, another simulation on the second adapted grid was performed. A transient period was allowed to equalize the number of incoming and outgoing molecules from the DSMC domain before flow field and surface sampling began. The simulation required about seventeen million molecules with 7600 steady state time steps to provide a good statistical database. Program execution required 2,081.6 node hours on SGI R10000 CPUs and used about 370 Mwords of computer memory. The solution of this jet interaction simulation is compared with the CFD solution in the section below.

Comparison between CFD and DSMC

Given in this section is a comparison between results obtained from the CFD and the uncoupled CFD-DSMC flow solutions for the interaction of a sonic argon jet at a plenum pressure of 34.5 kPa with the rarefied nitrogen free stream. The comparison between the two numerical techniques is made using flow field streamlines, number density contours, and surface pressure and heating on the symmetry plane and at three cross flow planes spanning the jet nozzle location.

Symmetry Plane

Flow field streamlines of the jet interaction on the symmetry plane from the CFD solution are shown in Fig. 3 and from the DSMC solution are shown in Fig. 12. Note that the flat plate and jet outgassing surface in Fig. 12 are shown as an outline to highlight the position of the jet outgassing surface on the upper flat plate surface. Free stream flow is from left to right and the sonic jet is injected from the upper flat plate surface 0.125 m from the sharp leading edge.

The jet gas injected at the flat plate surface acts as a three-dimensional protuberance to the incoming free stream. Two noticeable counter rotating vortices (shown in streamline Figs. 3 and 12) are located within a forward separation region on the upper flat plate surface just upstream of the injected jet. A primary forward vortex turns the free stream flow above the local jet interaction region, and a jet induced vortex (just aft of the primary) entrails the jet gas. These effects are shown by the vortex streamlines in Figs. 3 and 12 just above the upper plate surface and upstream of the nozzle exit. Also, the figures show that the primary forward vortex entrains a portion of the injected jet gas, as evidenced by the streamlines that start in the nozzle for the CFD solution and on the jet outgassing surface for the DSMC solution, pass above the jet induced vortex and are incorporated into the primary forward vortex.

The streamlines of both Figs. 3 and 12 also show that the nozzle flow has a prominent influence on the upper free stream flow streamlines. The flow above the flat plate is turned and the streamlines are compressed by the nozzle jet. Flow turning of the free stream caused by the jet is maintained until the flow exits the computational domain. Likewise, the jet flow streamlines are compressed by the interaction with the free stream. Those streamlines, which are not brought forward into the jet induced vortex, are abruptly turned downstream by the free stream interaction. Also, flow directly behind the jet on the symmetry plane is at a lower pressure than the boundary layer flow beneath the plate as evidenced by the lower plate boundary layer streamlines turning upward through the plate wake region. Although pressure in the wake region is very low and may make the CFD solution invalid, a comparison between the CFD and DSMC streamlines

results show a good agreement in the location and flow direction in the plate wake region.

A comparison between the CFD and DSMC normalized number density contours on the symmetry plane is given next by Figs. 4 and 13, respectively. The same flow field features exist for both the CFD and DSMC solutions. The nitrogen free stream inflow condition is about four orders of magnitude less dense than the standard number density. As the free stream encounters the upper flat plate surface, it is initially compressed by the plate leading edge shock wave caused by the boundary layer displacement. Over the upper portion of the flat plate, the gas density initially decreases as a boundary layer develops and the gas temperature near the wall increases from viscous dissipation. The density of the near wall gas then increases at the forward separation region as it recompresses before either being directed above the separation region or entrained into the primary forward vortex upstream of the jet.

For the CFD solution shown as Fig. 4, as the jet flow leaves the nozzle exit, the constant number density contours are initially symmetric and show further jet expansion from the nozzle exit. Likewise, just outside the jet outgassing surface of the molecular simulation the jet flow expands (see Fig. 13). However, as the jet flow encounters the free stream flow, it compresses as shown by the higher number density region just above the jet. This higher density region is caused by the interaction between the free stream flow and jet. As discussed previously, the jet flow turns the free stream. The resultant compression can be seen on the figures as the curved upper number density contour, which intersects the computation domain near the intersection of the upper and downstream outflow boundaries. However, number density in the region downstream of the nozzle exit just above the flat plate surface decreases with distance indicating a low pressure wake has formed behind the jet and high density interaction compression region.

Number density contours below the plate for both the CFD and DSMC flow solutions show the influence of the underside compression surface. Flow beneath the plate is initially compressed by the underside shock wave; however, as the flow passes the intersection between the lower compression surface and free stream aligned surface, it expands and the number density decreases. The flow then exits either through the lower or downstream computational boundary.

Surface pressure and heating from the CFD and DSMC solutions on the symmetry line of the upper flat plate surface are compared next. Surface pressure is given in Fig. 14(a) and surface heat flux in Fig. 14(b). The CFD results are shown by a solid line, DSMC results by a dashed line. Pressure is normalized by the free stream momentum flux and heat flux is normalized by twice the free stream kinetic energy flux. The heat flux vector is positive for heat flow to the plate surface and negative for heat flow from the plate surface. This normalization and heat flux vector direction convention is used for all subsequent results.

As the free stream flow encounters the plate leading edge, a boundary layer develops. The CFD and DSMC results differ in this leading edge region. CFD predicts higher leading edge pressure and heating than does the DSMC. The CFD finite volume approximation at the leading edge calculates a thin boundary layer with a large boundary layer displacement change because a no slip wall condition is applied; however, the DSMC method does not impose the no slip wall condition. Because the flow near the sharp leading edge is rarefied, the DSMC results provide a better prediction in the near leading edge region than those of the CFD solution.

The levels of heating and pressure just downstream of the leading edge to the forward separation region (see streamline Figs. 3 and 12) are nearly identical as shown by Fig. 14. This indicates a high degree of confidence that both the CFD and DSMC methods are predicting the actual pressure and heating in this region.

As the local flow over the plate encounters the forward separation region, it is turned away from the plate and compressed. A difference of less than 0.01 m in the location where the pressure rises is shown between the CFD and DSMC results. The CFD solution gives a pressure rise closer to the leading edge than the DSMC result. In the forward separation region, the maximum surface pressure occurs close to the vortex reattachment point and is influenced by both the free stream compression from the jet interaction above and the flow impingement at the reattachment of the forward primary and jet induced vortices. Again, a difference is shown between the CFD and DSMC prediction. Maximum pressure in the forward separation region is greater for the DSMC result.

As shown in Fig. 14(b), with increasing distance from the leading edge, heating in the forward separation region first decreases under the primary forward vortex region, then increases to the vortex reattachment location. One possible explanation is that the primary forward vortex gains kinetic energy by momentum transfer from the free stream as it traverses the upper portion of its path. An energy balance occurs between the primary forward and jet induced vortices during the path down toward the reattachment point. Energy is then transferred as heat flux to the wall as the vortical flow traverses from the reattachment point to the point of separation from the surface, thus producing the

heating profile shown in Fig. 14(b). A comparison between the CFD and DSMC results shows surface heating is larger for the DSMC.

The CFD results of Fig. 14(a) show that jet flow influences the surface pressure just upstream and downstream of the nozzle near the exit because the nozzle is well under expanded. That is, the nozzle exit pressure is much greater than the free stream static pressure. Both upstream and downstream of the nozzle exit, the flow expands along the surface of the plate. Flow upstream of the nozzle exit is compressed as it is turned and entrained into the jet induced vortex. Downstream of the nozzle exit, the flow continually expands to the flat plate trailing edge. The near nozzle CFD heat transfer solution (see Fig. 14(b)) has a negative sign. As the argon jet is expanded from a plenum temperature of 300K, the gas temperature decreases. Because the wall of the plate is held at a constant temperature of 300K for the CFD solution, the lower temperature jet gas has heat transferred to it from the wall after exiting the nozzle, thus the negative heat transfer near the nozzle. This near nozzle effect is not captured by the DSMC solution. The Cartesian grid resolution and surface triangulation of the DSMC may not be sufficient at the base of the jet outgassing surface. However, because the effect is localized to the nozzle exit, the DSMC solution should not be substantially affected.

Cross Flow Plane at x = 0.100 m

Cross flow plane results from the CFD and DSMC solutions are presented next. The figures for these comparisons are arranged so that the CFD results are on the left-hand side and the DSMC results are on the right-hand side. A mirror of the y-coordinate direction and v-velocity component of the CFD solution was performed so that the side-by-side comparison between the CFD and DSMC results could be made on the same figure.

Shown on Figs. 15(a), (b), and (c) are the cross flow streamlines above the upper plate surface, number density contours, and surface pressure and heating comparisons, respectively, for the CFD and DSMC results at the plane perpendicular to the free stream flow direction, 0.100 m from the leading edge of the flat plate. The streamline and number density figures show the computational domain for each of the solutions. Note also, the open region below the z = 0.000 m location is the flat plate cross section. Surface pressure and heating given in Fig. 15(c) are the results on the upper flat plate surface.

Generally, similar streamlines are shown for the CFD and DSMC results in Fig. 15(a). A difference does exist near the juncture of the flat plate and symmetry plane (y, z ≈ 0.000 m); the CFD results show an upward streamline direction, but the DSMC results show a downward flow direction. As discussed earlier, the CFD solution predicts that the separation region forward of the jet is larger than that of the DSMC. The primary forward vortex center is located upstream of the x = 0.100 m location for the CFD, and downstream of the x = 0.100 location for the DSMC. (Compare Figs. 3 and 12.) Thus, the difference in streamline direction is consistent with predicted location of the primary forward vortex for each method.

Overall similar number density contours are shown at the cross flow plate for the CFD and DSMC solutions in Fig. 15(b). One noticeable difference though is that the gradient in CFD number density contours is displaced further from the plate surface than those from the DSMC. The CFD solution may have over estimated the boundary layer displacement at the sharp leading edge because of the no slip wall condition. This would cause a larger displacement of the leading edge compression wave from the plate surface and affect the number density contours as shown by the figure.

Surface pressure and heating at the x = 0.100 m location is given as Fig. 15(c). Both the CFD and DSMC results show a rise in pressure from the plate side wall to the centerline. However, the maximum pressure of the CFD is greater than that of the DSMC solution. Because the CFD streamlines shown in Fig. 15(a) near the symmetry plane are directed down toward the flat plate and the DSMC streamlines are directed upward, surface pressure near the symmetry plane would be different, with the CFD result greater than the DSMC. Also, Fig. 15(c) shows that heating follows the same trend as the pressure in the cross flow direction; that is, heating rises from the plate side wall location to the plate centerline where it is a maximum. The heating maximum value is nearly the same for the CFD and DSMC solutions.

Cross Flow Plane at x = 0.125 m

Flow streamlines, number density contours, and surface pressure and heating at the cross flow plane that bisect the jet nozzle at x = 0.125 m are given next in Figs. 16(a), (b), and (c), respectively. Flow streamlines from the CFD and DSMC solutions show that the jet gas has replaced the free stream boundary layer at this cross section because flow streamlines over the region closest to the upper plate surface begin at either the nozzle plenum (CFD) or from the jet outgassing surface (DSMC) and track to the side of the computational domain or upward where the flow is convected down stream by the free stream flow. Also, a vortical flow region, just above the flat plate and at nearly the same distance from the symmetry plane, is present for both

solutions. The jet induced vortex (just upstream of the jet nozzle on Figs. 3 and 12) has turned about the jet and emerges from this cross flow plane as the vortex structure shown in Fig. 16(a).

Number density contours at the x = 0.125 m plane are shown as Fig. 16(b). Note the number density contour figure (Fig. 16(b)) shows the jet nozzle on the left-hand side (CFD) and the jet outgassing surface on the right-hand side (DSMC). A complex flow interaction region is shown above the jet injection. Jet flow from either the nozzle plenum or jet outgassing surface expands outward until being compressed by the interaction with the free stream. The interaction causes a rise in number density as the jet and free stream flow are compressed and turned from the original flow direction. The DSMC solution shows larger gradients in the compression region above the jet nozzle, thus producing a solution with stronger shock waves in the interaction than that of the CFD solution. The DSMC symmetry plane number density contours of Fig. 13 also show stronger interaction compression than those of the CFD solution shown as Fig. 4.

Pressure and heating at the cross flow plane are presented next as Fig. 16(c). Pressure and heating rise from the plate side value to a maximum and then fall with decreasing distance to the nozzle at the symmetry plane. Maximum pressure and heating occurs for both the CFD and DSMC solutions about 0.030 m outboard of the nozzle. This y location corresponds generally to the wall reattachment region of the vortex just above the plate surface shown on Fig. 16(a). Note that the maximum pressure and heating of the DSMC solution are higher than the CFD level. Also, the near nozzle CFD pressure results show the expanding flow of the jet as a large pressure spike. This was also observed with the CFD solution presented as Fig. 14(a).

Cross Flow Plane at x = 0.150 m

The final cross flow plane comparison of streamlines, number density contours, and surface pressure and heating is given at the plate trailing edge as Figs. 17(a), (b), and (c), respectively. Flow streamlines show that the vortices of the previous cross flow plane (see Fig. 16(a)) persist to the plate trailing edge; however, the vortices become elongated and less organized rising further above the flat plate surface because of mixing as angular momentum is transferred to the surrounding fluid. Also, flow at the symmetry plane is directed upward away from the plane surface as the upward jet injection still affects the flow at the trail edge cross flow plane.

The number density contours at the x = 0.150 m location are given as Fig. 17(b). The same features are shown for both the CFD (left-hand side) and the DSMC (right-hand side) flow field solution. The jet interaction region has become larger about the symmetry plane. Both solutions show a high density lobe corresponding to vortex reattachment location, shown in Fig. 17(a), which is larger and more diffused than at the x = 0.125 m cross flow plane. (See Fig. 16(b).) Note that the DSMC solution domain did not extend far enough from the upper plate surface to capture the entire density gradient field of the interaction. However, the number density contours given on the right-hand side of the figure show that most of the flow features have been captured by the DSMC solution.

Surface pressure and heating, similar to the results at the x = 0.125 m cross flow plane of Fig. 16(c), are shown in Fig. 17(c) at the plate trailing edge cross flow plane. Surface pressure and heating rise to a maximum near the vortex reattachment and fall with decreasing distance to the symmetry plane. Although surface pressure and heating of the DSMC solution is higher than CFD results, the difference is less than at the nozzle cross flow plane.

Conclusions

CFD and DSMC solutions have been obtained for an experimental test condition of a continuum sonic jet interacting with the rarefied flow about a sharp leading edge flat plate at zero incidence. Results on the symmetry plane and at cross flow planes spanning the jet injection location show a good quantitative flow field comparison based on flow streamlines and number density contours. Both CFD and DSMC predict counter rotating vortices forward of the jet injection region. In regions of high density vortex reattachment, CFD and DSMC solutions differ, the DSMC solution gives maximum pressure and heating values higher than those of the CFD.

A set of guidelines was developed to define the boundary between the jet and free stream interaction interface to uncouple the continuum jet from the interaction region. Using the guidelines, an uncoupled CFD-DSMC solution was obtained. The uncoupled solution method better utilizes computational resources by applying the continuum flow analysis to the continuum portion of the jet and the molecular flow analysis to the interacting flow field.

Acknowledgements

Contributions during the course of this research are acknowledged below. Mr. William Bene of the NASA Langley GEOLAB converted the EnSight™ breakdown surface cloud of points to an IGES format using the Surfacer program. Ms. Karen Bibb assisted with the use of the GridTool and FELISA programs.

Discussions with Drs. Richard Wilmoth, James Moss, Didier Rault, and Graeme Bird provided an enhanced understanding of the DSMC technique and application of the technique to an interacting flow.

Disclaimer

The use of commercially available software for this research does not represent an endorsement of the software by the U. S. Government.

References

[1]Romere, Paul O., Kanipe, David B., and Young, James C., "Space Shuttle Entry Aerodynamic Comparisons of Flight 1 with Preflight Predictions," *Journal of Spacecraft and Rockets*, Vol. 20, January-February 1983, pp. 15-21.

[2]Kanipe, David B. and Roberts, Barney B., "Evolution of the Wind Tunnel Test Program for Space Shuttle Orbiter Jet Interaction upon Entry and Comparison of Predictions with Flight Test Results," CPIA Publication 357, JANNAF 13th Plume Technology Meeting, Vol. 1, April 27-29, 1982, pp. 83-94.

[3]Throckmorton, David, "Today's technology for tomorrow's launch vehicles," *Aerospace America*, Vol. 33, No. 6, June 1995, pp. 20-24.

[4]Rault, D. F. G., "Aerodynamic Characteristics of the Magellan Spacecraft in the Venus Upper Atmosphere," *Journal of Spacecraft and Rockets*, Vol. 31, No. 4, July-August, 1994, pp. 537-542.

[5]Rault, D. F. G., Cestero, Francisco J., and Shane, Russell W., "Spacecraft Aerodynamics during Aerobraking Maneuver in Planetary Atmospheres," AIAA paper 96-1890.

[6]Allègre, J., Raffin, M., and Caressa, J. P., "Experimental Investigation of Transverse Jet Effects Related to Hypersonic Space Vehicles," *Aerothermodynamics for Space Vehicles*, Proceedings of the First European Symposium, ESTEC, Noordwijk, The Netherlands, 28-30 May 1991, ESA-SP-318, July 1991, pp. 165-170.

[7]Gilmore, Martin R. and Warburton, K., "Axi Symmetric Hypersonic Jet Interaction: A Combined Experimental and Computational Study II," AIAA paper 95-0414.

[8]Gilmore, Martin R., personal communication, August, 1996.

[9]Wilmoth, Richard G. and Tartabini, Paul V., "Three-Dimensional DSMC Calculations of Jet/Corner Flow Interactions," Presented at the 19th International Symposium on Rarefied Gas Dynamics, Oxford University, Oxford, England, July 25-29, 1994.

[10]Tartabini, Paul V., Wilmoth, Richard G., and Rault, Didier F. G., "Direct Simulation Monte Carlo Calculation of a Jet Interaction Experiment," *Journal of Spacecraft and Rockets*, Vol. 32, No. 1, January-February 1995, pp. 75-83

[11]COESA, "The U. S. Standard Atmosphere, 1976," NOAA, NASA, USAF, NOAA-S/T 76-1562, Washington, D. C., October 1976.

[12]McGrory, William D., Slack, David C., Applebaum, Michael P., and Walters, Robert W., "GASP Version 2.2 The General Aerodynamic Simulation Program," AeroSoft, Inc., 1993.

[13]AeroSoft, "GASP Version 3, The General Aerodynamic Simulation Program, Computational Flow Analysis Software for the Scientist and Engineer, User's Manual," AeroSoft, Inc., Blacksburg, Virginia, May 23, 1996.

[14]Bird, G. A., *Molecular Gas Dynamics*, Clarendon Press, Oxford, 1976.

[15]Bird, G. A., *Molecular Gas Dynamics and the Direct Simulation of Gas Flows*, Clarendon Press, Oxford, 1994.

[16]Wilmoth, Richard G., LeBeau, Gerald J., and Carlson, Ann B., "DSMC Grid Methodologies For Computing Low-Density, Hypersonic Flows About Reusable Launch Vehicles," AIAA paper 96-1812.

[17]Borgnakke, C. and Larson, P. S., "Statistical Collision Model for Monte Carlo Simulation of Polyatomic Gas Mixtures," *Journal of Computational Physics*, Vol. 18, No. 4, 1975, pp. 405-420.

[18]Message Passing Interface Forum, "MPI: A Message-Passing Interface Standard," Computer Science Department Technical Report CS-94-230, University of Tennessee, Knoxville, TN, 1994.

[19]Ohio Supercomputer Center, "MPI Primer / Developing with LAM," The Ohio State University, November 11, 1996.

[20]Lumpkin III, Forrest E., LeBeau, Gerald J., and Stuart, Phillip C., "A CFD/DSMC Analysis of Plumes and Plume Impingement during Shuttle/Mir docking," AIAA paper 95-2034.

[21]Rault, D. F. G., "Methodology for Thruster Plume Simulation and Impingement Effects Characterized Using DSMC," AIAA paper 95-2032.

[22]Walatka, Pamela P., Buning, Pieter G., Pierce, Larry, and Elson, Patricia A., "PLOT3D User's Manual," NASA Technical Memorandum 101067, March 1990.

[23]Computational Engineering International, Inc., "EnSight User Manual for Version 5.5.2," CEI, Research Triangle Park, North Carolina, 1996.

[24]Smith, Bradford, Rinaudot, Gaylen R., Reed, Kent A., and Wright, Thomas, "Initial Graphics Exchange Specification (IGES), Version 4," National

Bureau of Standards Report NBSIR 88-3813, published by The Society of Automotive Engineers, Inc., Warrendale, PA, June 1988.

[25]Imageware, Inc., “Surfacer User’s Guide,” SUR.UG./4-95, Ann Arbor, Michigan, 1995.

[26]Samareh, Jamshid, "GridTool: A Surface Modeling and Grid Generation Tool," Proceedings of the Workshop on Surface Modeling, Grid Generation, and Related Issues in CFD Solutions, NASA CP-3291, May 9-11, 1995.

[27]Peiró, J, Peraire, J, Morgan, K., “FELISA SYSTEM, Version 1.1, Reference Manual, Part 2-User Manual,” Tech. Rep., University of Swansea Report, August 5, 1994.

[28]Moss, James N., Rault, Didier F. G., and Price, Joseph M., “ Direct Monte Carlo Simulations of Hypersonic Viscous Interactions Including Separation,” Rarefied Gas Dynamics: Space Science and Engineering, *Progress in Astronautics and Aeronautics*, Vol. 160, AIAA, Washington DC, 1993.

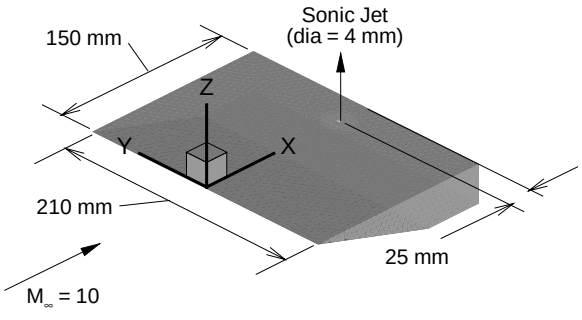

Fig. 1. Schematic diagram of the jet interaction flat plate model.

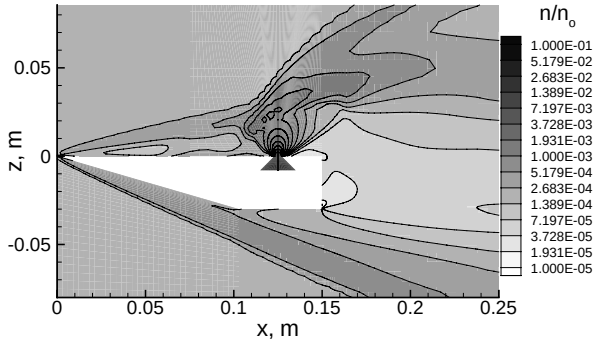

Fig. 4. Number density contours on the symmetry plane from the CFD solution.

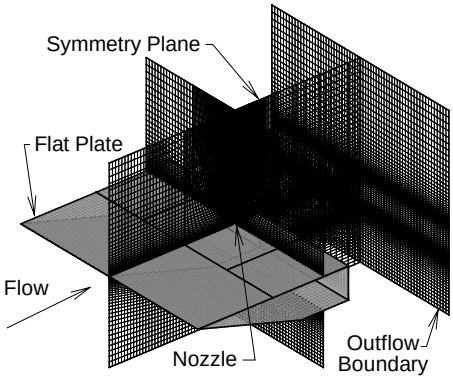

Fig. 2. Selected grid planes of the CFD computational domain.

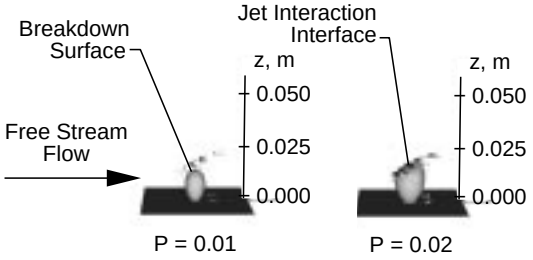

Fig. 5. Jet breakdown surface from CFD solution (P is the Bird breakdown parameter).

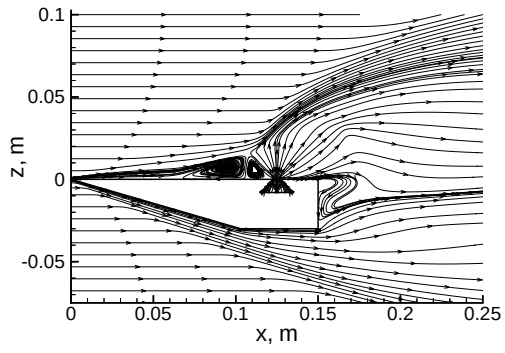

Fig. 3. Flow field streamlines on the symmetry plane from the CFD solution.

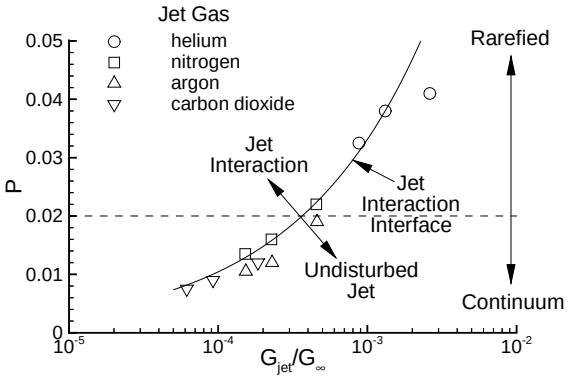

Fig. 6. Correlation of breakdown parameter value at breakdown surface interface with jet interaction.

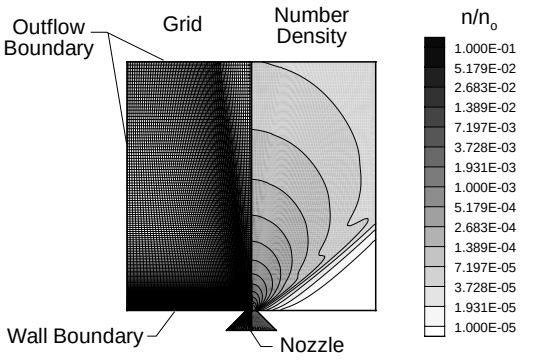

Fig. 7. CFD grid and number density contours for axi-symmetric free expanding jet.

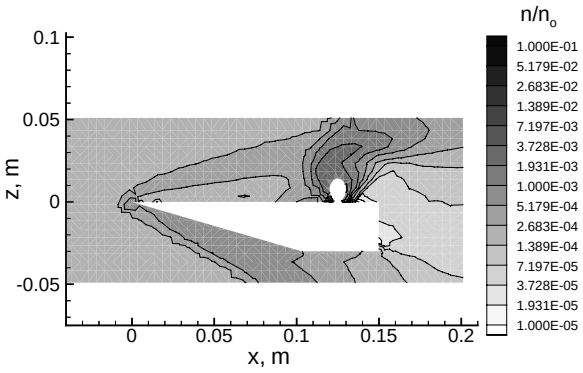

Fig. 10. Number density contours on the symmetry plane from the uniform grid DSMC solution.

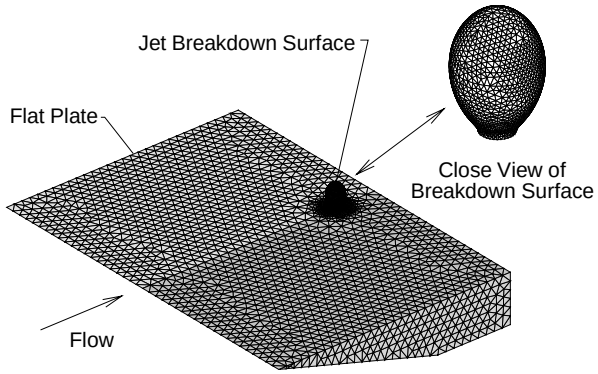

Fig. 8. Triangulated flat plate and jet outgassing surface geometries.

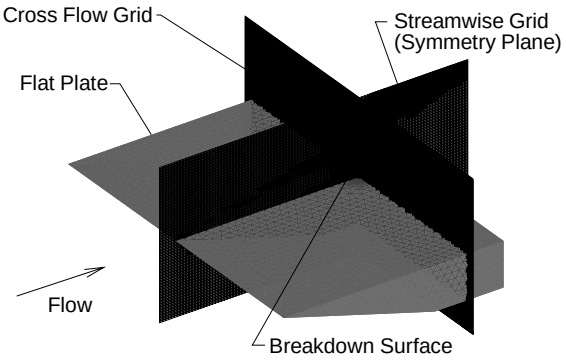

Fig. 11. DSMC adapted grid for the jet interaction problem.

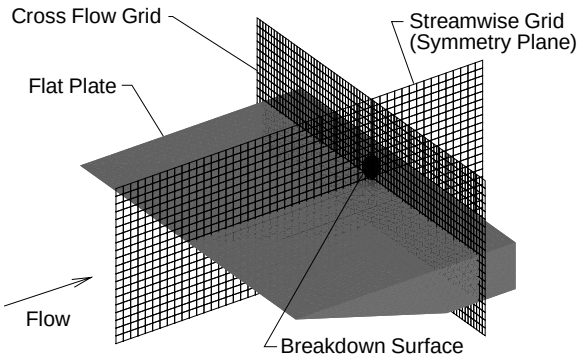

Fig. 9. DSMC uniform grid for jet interaction problem.

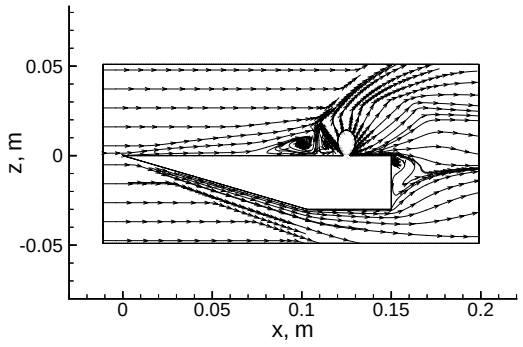

Fig. 12. Flow field stream lines on the symmetry plane from the adapted grid DSMC solution.

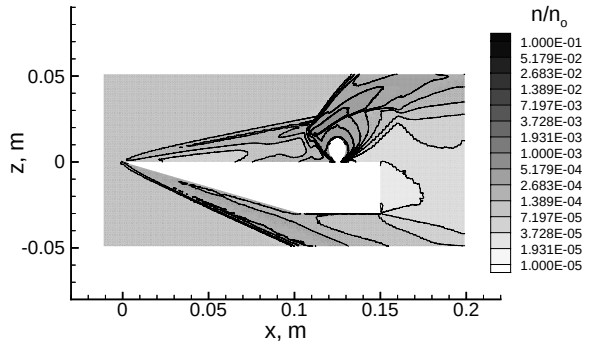

Fig. 13. Number density contours on the symmetry plane from the adapted grid DSMC solution.

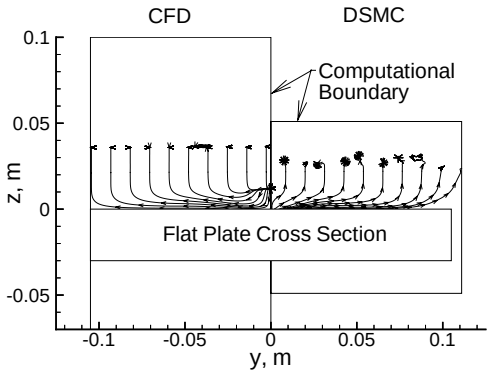

(a) Flow field streamlines

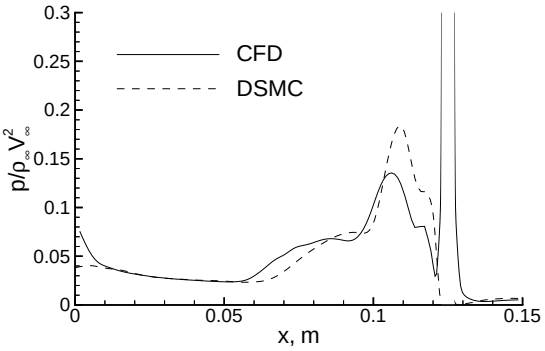

(a) Surface pressure.

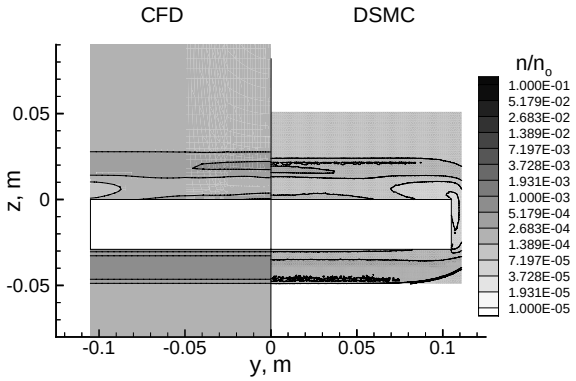

(b) Flow field number density contours.

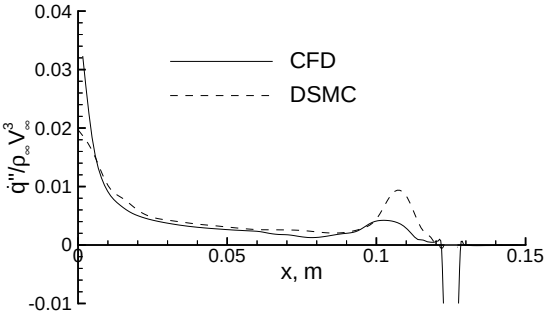

(b) Surface heating.

Fig. 14. Comparison between CFD and DSMC on the symmetry line.

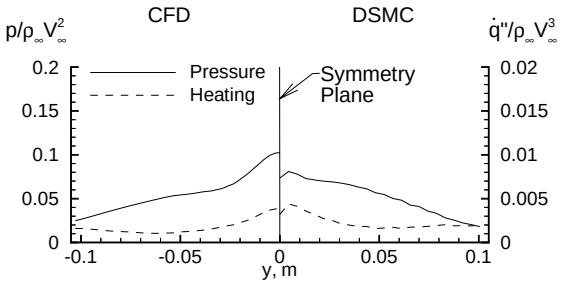

(c) Surface pressure and heating.

Fig. 15. Comparison between CFD and DSMC at the x = 0.100 m cross flow plane.

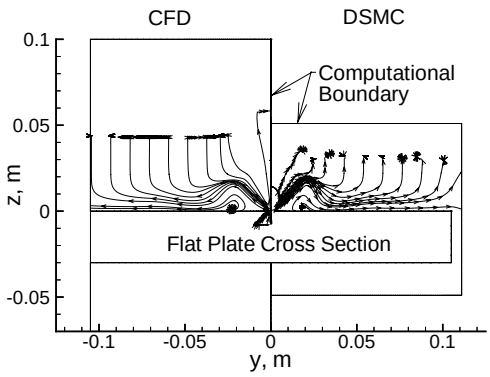

(a) Flow field streamlines.

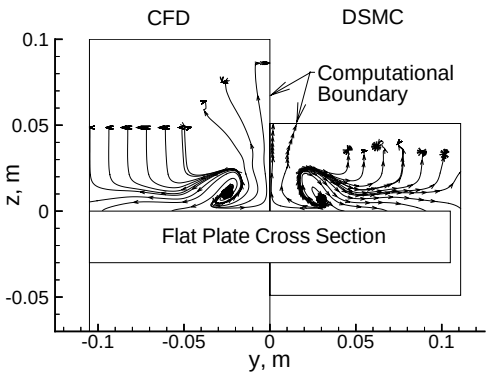

(a) Flow field streamlines.

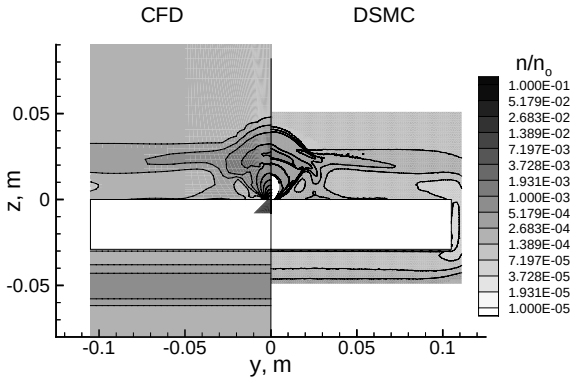

(b) Flow field number density contours.

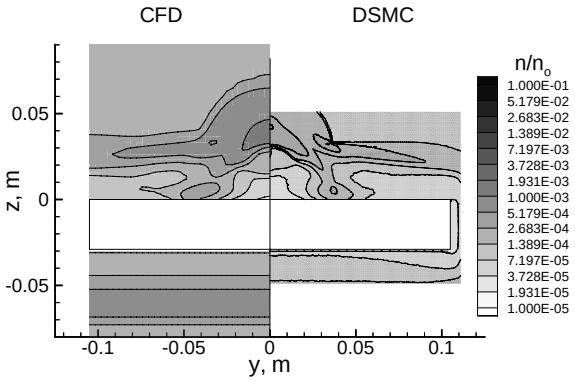

(b) Flow field number density contours.

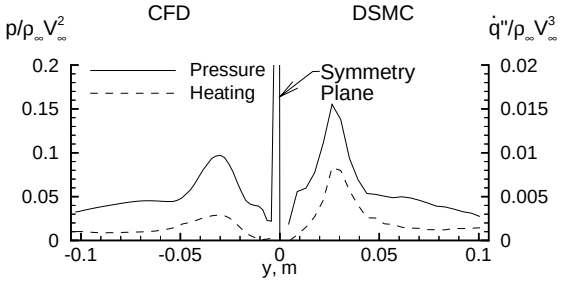

(c) Surface pressure and heating.

Fig. 16. Comparison between CFD and DSMC at the x = 0.125 m cross flow plane.

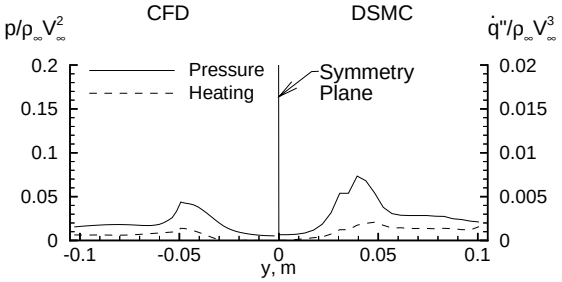

(c) Surface pressure and heating.

Fig. 17. Comparison between CFD and DSMC at the x = 0.150 m cross flow plane.